RSC Advances

PAPER

View Article Online
View Journal | View Issue

Cite this: *RSC Adv.*, 2024, **14**, 24548

Unveiling the anti-corrosion properties of Zn-eggshell particle composite coatings on mild steel in seawater-simulated solution using starch as a modifier

Victor Sunday Aigbodion [abc] and Ekele Dinneya-Onuoha *[cd]

This study investigates the development and efficacy of Zn-eggshell particle (ESAp) coatings on mild steel, utilizing starch extract as a modifier to enhance anti-corrosion properties. Coatings with varying ESAp content (0, 2, 4, 6, and 8%) and a fixed addition of 2% starch were successfully applied *via* electrodeposition. The findings reveal that increasing the ESAp content results in thicker coatings, with the Zn-8% ESAp + 2% starch coating exhibiting the greatest thickness. SEM analysis confirmed the high quality of the coatings, showing no external surface defects. The Zn-8% ESAp + 2% starch-coated sample demonstrated a 46.45% increase in hardness (100.3 HB) and achieved superior corrosion protection efficiencies of 82.92% and 94.69% for Zn-8% ESAp and Zn-8% ESAp + 2% starch coatings, respectively. Electrochemical tests indicated that the coated samples shifted towards higher positive potential values, suggesting enhanced corrosion resistance. The results underscore the potential of using starch extract and waste eggshells to develop robust anti-corrosion coatings, with Zn-8% ESAp + 2% starch identified as the optimal formulation for superior protection and mechanical properties. Further research is recommended to explore the matrix–particle interactions and adhesion properties using advanced microscopic and electrochemical techniques.

Received 11th June 2024
Accepted 22nd July 2024

DOI: 10.1039/d4ra04283b

rsc.li/rsc-advances

1. Introduction

Effective corrosion prevention techniques have long been considered essential to materials science and engineering, especially in fields where metallic constructions are frequently exposed to harsh environmental conditions.[1–3] This is especially true in industries like construction, transportation, maritime, and oil and gas, where the integrity of metal structures is crucial to safety, usefulness, and lifespan.[4,5] The electrochemical process of corrosion, which occurs when metals deteriorate due to interactions with surrounding elements, endangers the structural integrity and aesthetic value of metals and results in large financial losses.[6–9] Globally, corrosion is thought to cost billions of dollars every year.[10] This cost includes direct costs such as maintenance and replacing corroded components, as well as indirect costs such as production downtime, lost efficiency, and environmental contamination.[10–12]

Zinc (Zn) and its derivatives are widely favored as protective coatings due to their excellent galvanic protection properties.[13–16] Acting as sacrificial anodes, zinc corrodes preferentially to the underlying metal, forming a robust protective barrier.[13,17,18] In steel construction, cathodic protection proves highly effective in preventing rust. Zinc coatings, similar to galvanization, have long been utilized for their cost-effectiveness, ease of application, and reliable performance across diverse conditions.[14] Despite their extensive use, potential enhancements through modifications and composite formulations offer significant promise for boosting effectiveness. While traditional zinc coatings perform adequately, they remain susceptible to environmental degradation, especially in harsh conditions characterized by high humidity, salt, and industrial contaminants.[19] Achieving greater mechanical strength, longevity, and corrosion resistance in these coatings necessitates the adoption of novel materials and hybrid manufacturing techniques.

Research now focuses on developing composite coatings, which combine zinc with other materials to provide protective layers with many uses.[20,21] Natural materials have garnered a lot of attention lately for use in engineering applications. This paradigm shift was prompted by the demand for long-term, ecologically conscious solutions that minimize environmental effects while preserving or enhancing material performance.[20]

[a]*Faculty of Engineering and the Built Environment, University of Johannesburg, P. O. Box 534, Auckland Park, South Africa*

[b]*Department of Metallurgical and Materials Engineering, University of Nigeria, Nsukka Postal Code 410001, Nigeria*

[c]*Africa Centre of Excellence, ACESPED University of Nigeria, Nsukka Postal Code 410001, Nigeria*

[d]*Department of Pure and Industrial Chemistry, University of Nigeria, Nsukka Postal Code 410001, Nigeria. E-mail: ekele.onuoha@unn.edu.ng*

Eggshell particles, a byproduct of the food industry, have emerged as a viable replacement for such uses.[22–24] Calcium carbonate ($CaCO_3$), the main component of eggshells, has natural qualities that can improve the mechanical strength and corrosion resistance of composite coatings.[23] Using eggshell particles in zinc coatings has several advantages. First, by sealing up micro-pores and other imperfections in the zinc matrix, calcium carbonate can act as a physical barrier to lessen the entry of corrosive substances.[25] $CaCO_3$ can also engage in chemical reactions that enhance the coating's protective properties.[26] For example, when moisture and CO_2 are present, calcium carbonate may transform into calcium bicarbonate, as shown by eqn (1).

$$CaCO_3 + CO_2 + H_2O \rightarrow Ca(HCO_3)_2 \quad (1)$$

This reaction raises the overall density of the coating and helps close micro-cracks. Moreover, acidic environments, which often intensify corrosion processes, can be countered by the alkaline properties of $CaCO_3$.[27] The neutralization process described in eqn (2) may take place when the coating is exposed to acidic conditions:

$$CaCO_3 + 2HCl \rightarrow CaCl_2 + CO_2 + H_2O \quad (2)$$

This neutralization can stop corrosion to the underlying metal by balancing the pH at the metal-coating contact.[27] To help create a more adherent and compact layer, eggshell particles are added to the mixture, increasing the layer's mechanical integrity and resistance to degradation. Aigbodion and Akinlabi[28] found that the zinc-eggshell particles composite coating on mild steel demonstrated better corrosion resistance and thermal stability than traditional zinc coatings. At a certain concentration of eggshell powder, the composite coating showed a notable improvement in corrosion resistance, achieving a maximum corrosion protection efficacy of 82.3%. Furthermore, microstructural alterations were discovered and the thermal properties of the composite coating were enhanced, both of which may result in increased adhesion and protective characteristics.

Eggshell particles are an excellent addition to zinc-based anti-corrosion coatings, however dispersion, adhesion, and homogeneity are still intrinsic issues with composite coatings. Recent research has examined several novel approaches to address the issues of dispersion, adhesion, and uniformity in composite coatings. By enhancing adhesion and dispersion, coupling agents and silanization—two sophisticated surface modification techniques—have increased the interfacial interaction between particles and the matrix.[29,30] Particle dispersion within the composite matrix has been shown to be enhanced by the inclusion of surfactants and dispersants, such as naturally occurring polymers like chitosan and gelatin.[31,32] Furthermore, the use of nanoparticles like graphene oxide and carbon nanotubes in the development of nanocomposite coatings has shown enhanced mechanical characteristics and homogeneity because of their strong interfacial contacts and high aspect ratios.[33–35] Additionally, it has been shown that during the production of composite coatings, high-shear mixing and ultrasonic agitation may be used to break up particle agglomerates and provide a more uniform distribution.[32,36] Furthermore, improvements to electrophoretic deposition protocols have allowed composite materials to be deposited more precisely and evenly, resulting in coatings with improved structural integrity and performance.[37–39] However these technologies also frequently entail difficult, expensive, and time-consuming procedures.[40] They could also need significant energy inputs or introduce potentially hazardous substances, which would make them less environmentally friendly and inappropriate for large-scale applications. On the other hand, starch offers a more straightforward, economical, and ecological alternative as it is a readily available, biodegradable, and non-toxic substance.

When starch was added to the electrolyte system, a denser and thicker oxide layer formed on the alloy surface compared to the electrolyte without starch, according to Kaseem and Ko's[41] analysis of the impact of starch on the corrosion behavior of Al–Mg–Si alloy processed *via* micro-arc oxidation (MAO). The alloy's resistance to corrosion in chloride conditions was enhanced by the denser oxide layer, which had a lower porosity and included both the γ-Al_2O_3 and α-Al_2O_3 phases. Compared to the alloy made without starch, the use of starch improved the structural qualities of the protective layer and enhanced its corrosion resistance. The study highlighted the possibility of using starch as an affordable and environmentally friendly additive to increase the corrosion resistance of MAO's Al–Mg–Si alloy coatings.

Akinfenwa *et al.*[42] claim that adding starch to Zn–TiO_2 coatings significantly improves their anti-corrosion properties. Compared to the unmodified Zn–TiO_2 coating, which corrodes at a rate of 6.7197×10^{-4} mm year^{-1}, the study discovered that Zn–TiO_2-starch coatings had significantly reduced corrosion rates, ranging from 4.1902×10^{-4} to 2.418×10^{-4} mm year^{-1}. The increased starch concentrations in the coating were thought to be responsible for its improved corrosion resistance due to improved starch granule dispersion as seen by SEM/EDS imaging and the creation of stable crystallite phases in XRD patterns. The starch-modified coatings provide a more homogeneous, hydrophobic barrier, which increases the coating's resilience to corrosive conditions.

The purpose of this study is to utilize electrodeposition to produce and evaluate a novel anti-corrosion coating incorporating zinc and starch-modified eggshell particles. Electrodeposition is a versatile and commonly employed process for depositing metallic coatings, offering precise control over coating microstructure, thickness, and composition.[43] This method is useful when metal matrices and particle reinforcements are co-deposited since it makes it possible to create composite coatings with specific characteristics.[44] The major goals are to examine the combined impact of these materials on the microstructural characteristics, mechanical capabilities, and corrosion resistance of the resulting coatings. This research aims to advance corrosion prevention through high-performance, environmentally friendly composite coatings. It leverages the inherent properties of eggshell particles and the

binding capabilities of starch. This finding is significant as it offers a sustainable alternative to conventional anti-corrosion coatings, thereby supporting global initiatives in materials engineering. The study's findings might lead to the development of novel coating formulae that combine the benefits of natural and engineered materials, producing corrosion prevention solutions that are more durable and eco-friendly.

2. Materials and method

2.1. Materials

The outcomes of this experiment could be relied upon since all chemicals used were of analytical grade. The primary materials were mild steel from Ajaokuta Steel in Nigeria and eggshells (ES) from Enugu State in Nigeria. The chemical analysis, displayed in Table 1, shows the elemental makeup of the mild steel and its suitability for this inquiry. The starch required to modify the anti-corrosion coating was purchased at the local market in Nsukka, Nigeria. The materials utilized in this experiment were prudently selected and handled to ensure the precision and integrity of the outcomes.

2.2. Method

2.2.1. Eggshell particle (ESAp) and mild steel processing. With some slight adjustments, the synthesis of ESAp was carried out based on the protocols described by Nandiyanto *et al.*[45] and Wibowo *et al.*[46] After being first cleansed with deionized water, the raw eggshells were gathered and sun-dried for three days. Afterwards, KOH was used as the main digestive precursor and the dried eggshells were burnt to ash in an electric furnace. Sodium hydroxide and simple combustion were used in the current procedure's pretreatment phase. To be more precise, the ash was combined with 400 milliliters of 2.5 M sodium hydroxide and heated for four hours at 100 °C. After that, Whatman Filter paper No. 5 (47 mm) was used to sift the mixture. Following titration of the residues, the mixture was stirred for eighteen hours to achieve a neutral pH in preparation for further purification. Two milligrams of sulfuric acid were then added. Following the formation of the two distinct gel layers, the layers were centrifuged at 6000 g for five minutes to remove the pellet. The stirring was then stopped. After cleaning the pellet several times with ethanol and deionized water, it was oven-dried for thirty minutes at eighty degrees Celsius. The dried pellet was then ground into a fine powder using a mortar and pestle.

To get rid of any impurities and oxides on the surface, the mild steel was first immersed in a 10% HCl solution for ten minutes. Following the acid treatment, metallographic grit sheets and alumina paste were used to polish and grind the steel to produce a uniformly smooth surface. After rinsing the prepared steel samples in deionized water to remove any last bits of abrasive material, they were dried completely. To prepare the mild steel samples for coating application, they were finally chopped into 5 cm by 4 cm pieces.

Table 2 Coating thickness of the coated samples

	1st reading	2nd reading	3rd reading	Average reading μm
Zn-ESAp				
0% ESAp	91	92	99	94
2% ESAp	98	99	100	99
4% ESAp	104	105	104	103.3
6% ESAp	125	130	128	127.7
8% ESAp	124	130	130	128
Zn-ESAp + 2% Starch				
0% ESAp	94	95	99	96
2% ESAp	99	99	100	99.3
4% ESAp	106	107	104	105.67
6% ESAp	130	130	128	129.3
8% ESAp	135	130	130	131.6

2.2.2. Composite fabrication. The new composites were made *via* the electrodeposition technique. The electrodeposition bath was prepared with 5 g L^{-1} thiourea, 100 g L^{-1} $ZnCl_2$, 15 g L^{-1} boric acid, and 100 g L^{-1} KCl. Starch concentration of 2% was combined with varying doses of ESAp at 0%, 2%, 4%, 6%, and 8%. To guarantee uniformity, the bath solution was constantly stirred throughout the day employing an aquarium pump and a magnetic stirrer. For twenty minutes, the electrodeposition operation was carried out with a current density of 2.5 A cm^{-2}. The electrodes were connected to a direct current source by a rectifier, with the substrate serving as the cathode and zinc metal serving as the anode.

2.2.3. Characterization. The coating thickness was ascertained by cutting perpendicular to the sample's length at a moderate speed with an Allied High Tech TechCut 4. Three independent measurements were averaged to determine the thickness of each sample to guarantee consistency and accuracy in the results.

The VeecoDektak 150 Profilometer was used to measure the surface roughness of the coatings. This gadget captures and amplifies the vertical displacements of a stylus moving at a constant rate across the sample surface to find surface irregularities. For this experiment, a stylus with a tip radius of 12.5 μm was employed, scanning at a speed of 26.7 μm s^{-1} with a force of 5 N. This method produced detailed surface topography data for the coatings.

To gather comprehensive details on the materials' chemical makeup and crystalline structure, X-ray diffraction (XRD) was utilized. CuKα radiation ($\alpha = 1.5418$ Å) at 34 kV and 25 mA was used to study the XRD patterns. An "X-PertProPANalytical, LR 39487C XRD diffractometer" was used for the experiments.

Table 1 Chemical composition of the mild steel used for this research (wt%)

Elements	C	Mn	Si	P	S	Zn	Al	Ni	Fe
%	0.16	0.35	0.15	0.0031	0.021	0.034	0.005	0.075	Balance

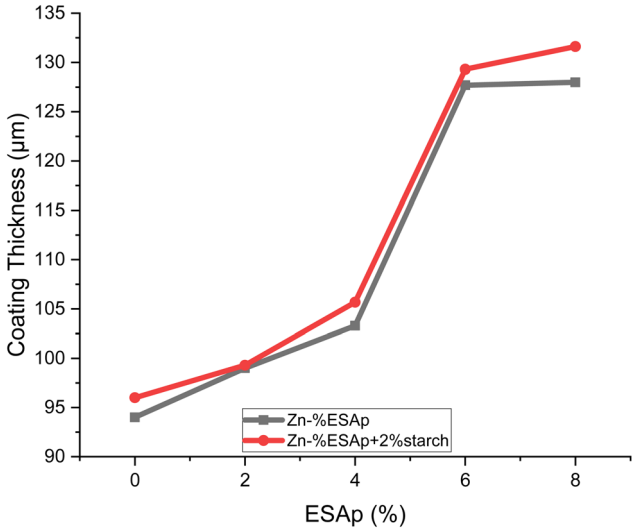

Fig. 1 Variation of surface roughness with %ESAp.

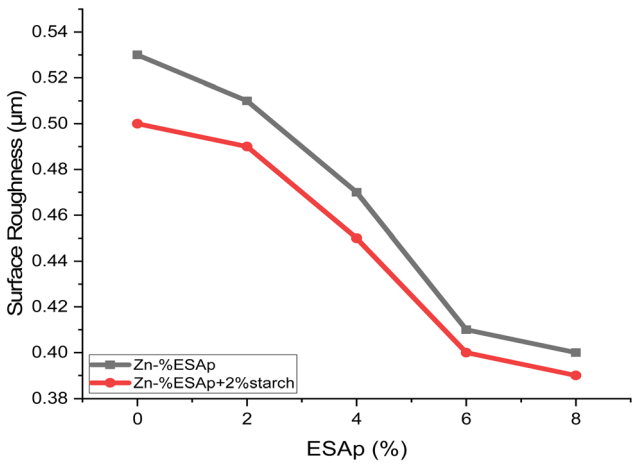

Fig. 2 Variation of surface roughness with %ESAp.

With step measurements made every 0.04° for 6 seconds per step, the diffraction data were acquired in a 2θ angular range spanning from 10 to 90°, yielding accurate and thorough crystallographic data.

TESCAN SEM was used to analyze the coated specimens' surface morphology (SEM). The specimens were carefully cleaned with acetone before imaging to guarantee a good view of the surface characteristics and eliminate any impurities. This cleaning process was necessary to avoid interference from residual particles that may obscure the coatings' true shape. The SEM analysis yielded high-resolution images of the specimens that allowed for a detailed inspection of the coating uniformity, surface structure, and any potential microstructural features. This inspection was necessary to assess the integrity and quality of the coatings and to comprehend their physical properties. The SEM images provided information on the distribution and microscopic interactions of the coating materials in addition to making it feasible to identify any faults, such as holes or cracks.

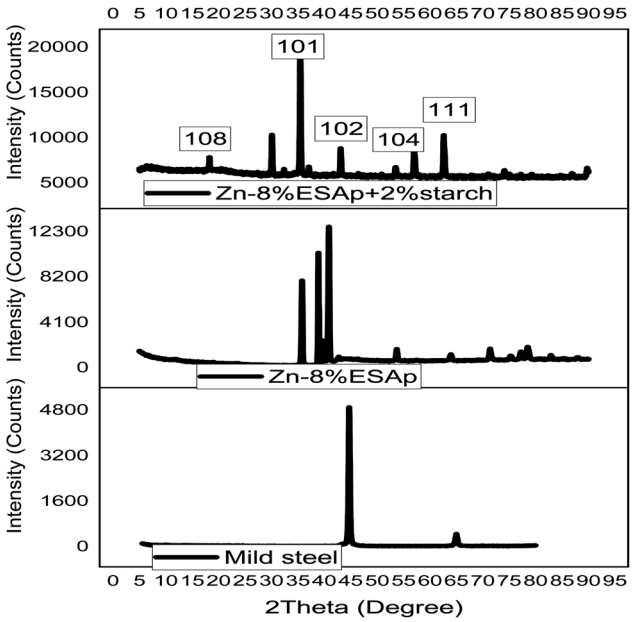

Fig. 3 XRD spectrum of the samples.

A portable Rockwell hardness tester was used to measure the hardness values of the coated specimens, strictly according to the ASTM E-384 hardness test methodology. A measurable indicator of the coating's resistance to deformation is provided by this established method, which guarantees accurate and consistent readings. An indenter was used in the test, and it was loaded to a certain point until it pierced the specimen's surface. The hardness value was obtained by measuring the indentation depth exactly. To ensure accuracy and reproducibility, this procedure was carried out repeatedly on each sample at various times in order to get the average hardness value.

The electrochemical tester, type CHI604E, was used to test for corrosion. The process guaranteed methodological precision and consistency by adhering to the ASTM G19 Standard. The reference electrode in the electrochemical setup was an Ag/AgCl electrode, the counter electrode was a graphite rod, and the working electrode was the coated samples. A 3.5% NaCl solution was utilized to replicate an environment that is corrosive, similar to seawater. In complete compliance with ISO 9227:2017 guidelines, the test settings comprised a potential range of 0.5 to −0.5 V, a temperature of 30 °C, a scanning rate of 0.5 mV s^{-1}, and a relative humidity (RH) of 100%. These circumstances guaranteed a regulated and repeatable setting for assessing corrosion behavior. Using the linear polarization eqn (1), the polarization resistance (RP) of the samples was determined, offering important information about the coatings' ability to protect. A thorough evaluation of the coated specimens' corrosion resistance and electrochemical stability was made possible by this extensive testing regimen.

$$R_P = \frac{\beta_a \beta_c}{2.3 i_{corr}(\beta_a + \beta_c)} \quad (3)$$

where; β_a and β_c are the anodic and Tafel constants and i_{corr} is the current density from the potentiodynamic curve.

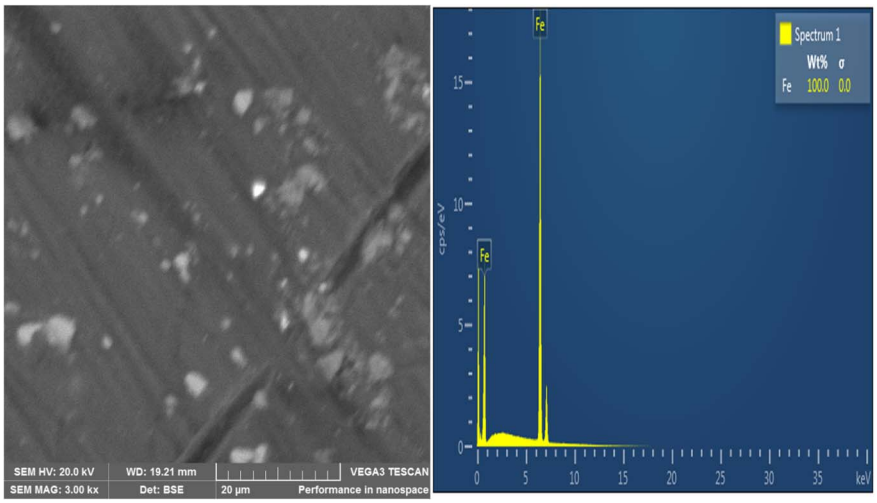

Fig. 4 SEM image of the mild steel.

3. Results and discussion

3.1. Coating thickness

Table 2 and Fig. 1 present the coating thickness data for the various samples and highlight noteworthy trends with the addition of eggshell particles (ESAp) and starch.

The samples with starch added had thicker coats than the ones without, per the results. Moreover, a rise in coating thickness was proportionate to an increase in the formulation's ESAp content. The sample containing 0% ESAp had the thinnest coating due to the absence of both starch and ESAp, highlighting the crucial role that both additives play in facilitating coating deposition. Interestingly, the Zn-8% ESAp + 2% starch coating exhibited the thickest layer of all the samples. This implies that starch and ESAp work in concert to promote a coating layer that is thicker and maybe more protective. Starch increased the viscosity of the electrodeposition solution, which resulted in a more uniform and dense deposition of zinc on the substrate, while ESAp, which is mostly made of calcium carbonate, served as nucleation sites for zinc deposition, encouraging a thicker coating. Since the deposition rate slowed down and became more regulated, the thicker coating was probably the result of the lower mobility of zinc ions caused by the greater viscosity.

3.2. Surface roughness (Ra)

The Ra values, which are shown in Fig. 2, after the deposition procedure provide important information on how starch affects the coatings. As depicted, the inclusion of starch markedly influences surface roughness. For instance, the surface roughness (Ra) values observed were 0.53, 0.51, 0.47, 0.41, and 0.40 μm for Zn-%*x*ESAp, and 0.50, 0.49, 0.45, 0.40, and 0.38 μm for Zn-%*x*ESAp + 2% starch, with *x* representing 0, 2, 4, 6, and 8 respectively. These results clearly indicate that the presence of starch significantly reduces both the grain sizes and the surface roughness of the coatings. Ra values decrease when starch is added, which is explained by the polymer's capacity to smooth out and improve the coated surface by refining the grain

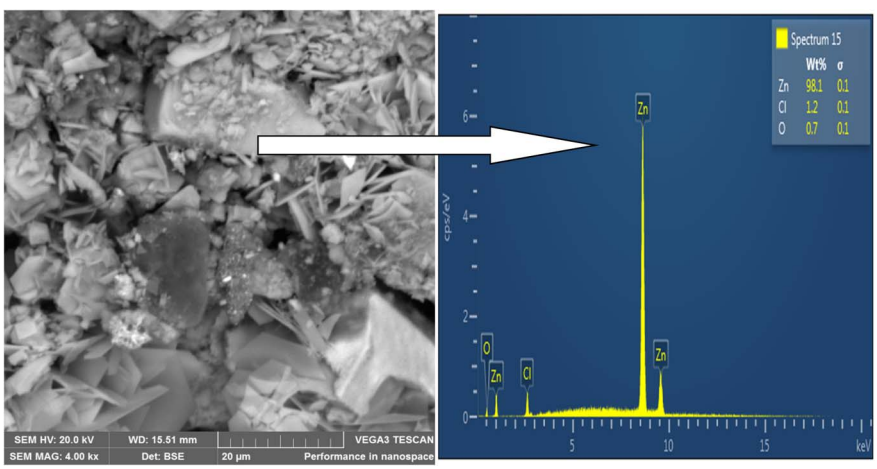

Fig. 5 SEM image of Zn-0% ESAp.

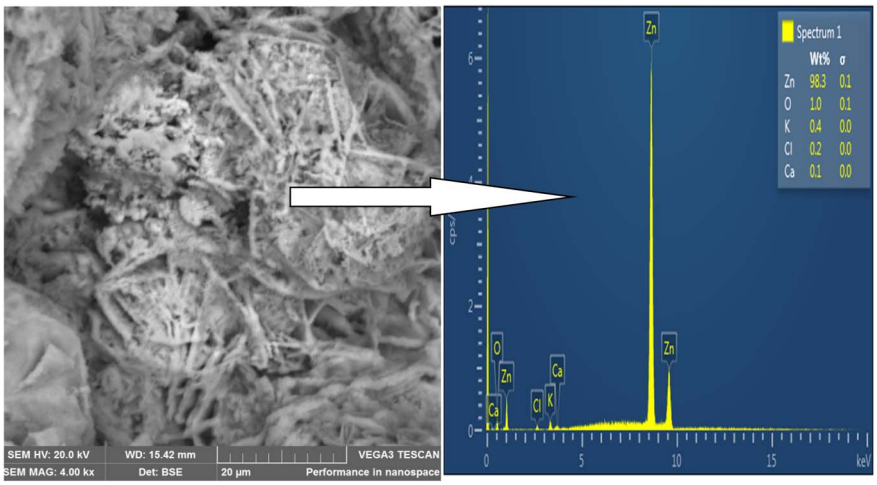

Fig. 6 SEM image of Zn-8% ESAp.

structure. Since reduced surface roughness is usually associated with increased resistance to corrosion and mechanical wear, this effect is very helpful for improving the protective qualities of the coatings.

3.3. X-ray diffraction analysis

Fig. 3 displays the XRD scans of the coated samples and the mild steel substrate. The substrate exhibited two prominent peaks at approximately 45 and 65°, corresponding to α-Fe and Fe_3C (101, 111) phases, respectively. After coating, the samples showed similarities to the substrate and notable extra peaks in their XRD patterns. The coated samples that included 8% ESAp and 8% ESAp + 2% starch, in particular, had distinct peaks at $2\theta = 45.5°$, suggesting the existence of Zn (102) and Fe_3C (101, 111) phases in addition to the α-Fe phase. The emergence of the Zn phase in the coated samples is caused by zinc's presence as the primary matrix component in the coating composition. This inclusion causes a Zn-rich layer to form on the mild steel surface, improving the coating's protective properties. The

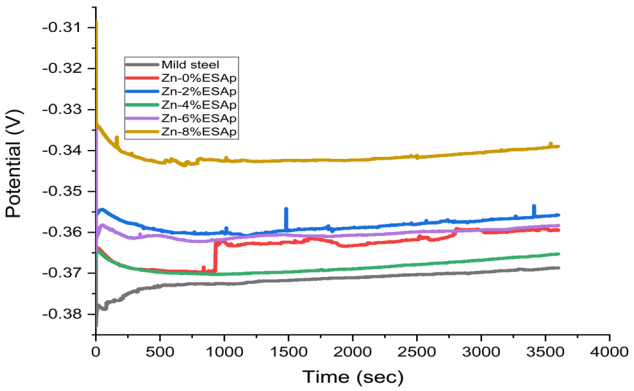

Fig. 8 OCP of the Zn-ESAp samples.

successful electrodeposition of the zinc-based composite coatings is confirmed by the presence of zinc in the XRD patterns. These results corroborate those of Fayomi *et al.*'s study,[47]

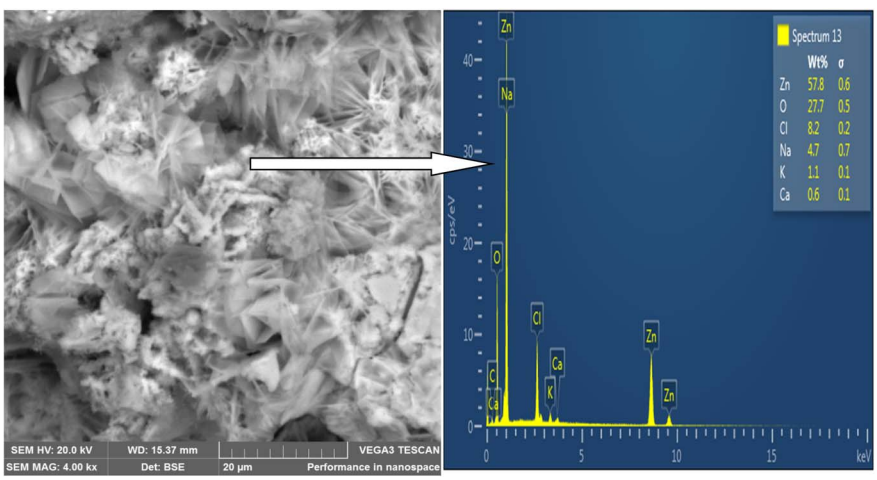

Fig. 7 SEM image of Zn-8% ESAp + 2% starch.

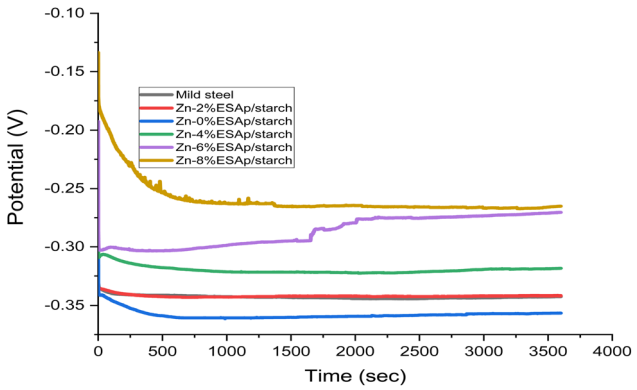

Fig. 9 OCP of the Zn-ESAp + 2% starch samples.

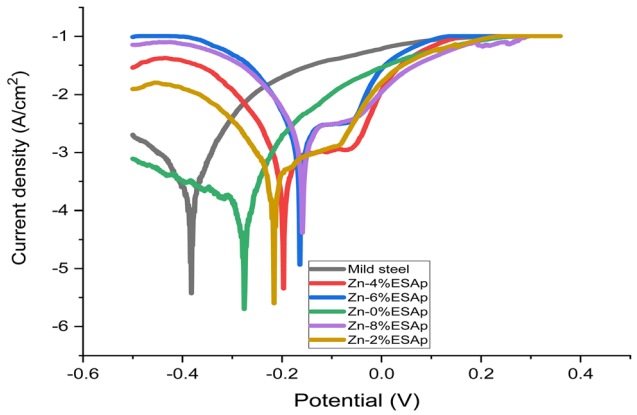

Fig. 10 Tafel extrapolation data of the Zn-ESAp samples.

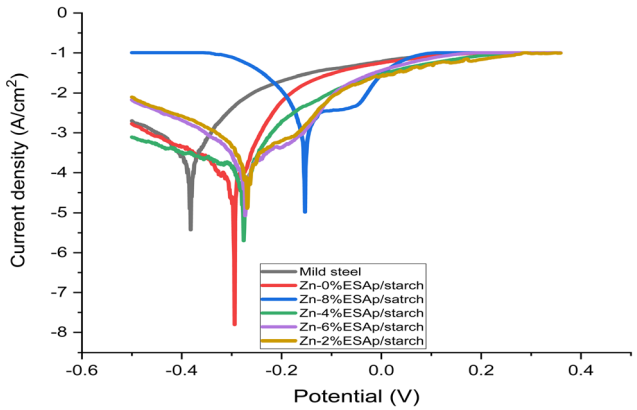

Fig. 11 Tafel extrapolation data of the Zn-ESAp + 2% starch samples.

demonstrating the value of zinc inclusion in enhancing the coatings' structural and protective qualities.

Moreover, large diffraction peaks at $2\theta = 40°$ and 51° were visible in the coated samples' XRD patterns, indicating the existence of the CaO and $CaSiO_3$ (100, 104) phases, respectively. These stages imply that the eggshell particles (ESAp) have a major impact on the system's crystalline behavior. These peaks' existence suggests that ESAp efficiently alters mild steel's

Table 3 Tafel results of the Zn-ESAp

Sample	Rate (mil per year)	Corrosion I (A)	Lin pol R (Ohms)
Mild steel	4.971×10^{2}	2.105×10^{-2}	10
0% ESAp	1.035×10^{2}	1.297×10^{-3}	31
2% ESAp	9.248×10^{1}	9.079×10^{-4}	46
4% ESAp	7.497×10^{1}	9.391×10^{-4}	42
6% ESAp	6.091×10^{1}	7.629×10^{-4}	50
8% ESAp	3.506×10^{1}	4.392×10^{-4}	99

Table 4 Tafel results of the Zn-ESAp + 2% starch

Sample	Rate (mil per year)	Corrosion I (A)	Lin pol R (Ohms)
Mild steel	4.971×10^{2}	2.105×10^{-2}	10
0% ESAp	8.472×10^{1}	1.061×10^{-3}	38
2% ESAp	7.003×10^{1}	8.773×10^{-4}	47
4% ESAp	5.335×10^{1}	6.682×10^{-4}	59
6% ESAp	3.389×10^{1}	4.245×10^{-4}	104
8% ESAp	2.638×10^{1}	3.304×10^{-4}	125

surface, encouraging the phases of calcium oxide and calcium silicate to develop within the coating. To improve the coating's mechanical and chemical qualities and increase its overall performance and longevity, this surface modification is essential.

In addition, Fig. 3 demonstrates that the coated sample containing 2% starch and 8% ESAp had more diffraction peaks and a lower interspacing distance than the 8% ESAp sample that was left untreated. This discovery implies that a more refined and densely packed crystalline structure results from the addition of starch to the ESAp composite. The interfacial interactions made possible by the inclusion of ESAp in the coating mixture lead to the creation of the $CaSiO_3$ phase in the composite coating. A composite material with improved structural integrity and corrosion resistance is produced as a result of these interactions, which facilitate the integration of silicon and calcium from the ESAp into the zinc matrix. The results are consistent with research by Aigbodion *et al.*,[48] which found that adding ESAp improved coating characteristics in a comparable way. The improved phase formation and crystalline structure support the coating's overall efficacy in shielding the mild steel substrate from corrosive conditions.

3.4. SEM analysis

SEM was used to analyze the composite coating's microstructure; the findings are shown in Fig. 4–7. The abrasive cutter lines may be seen as surface scratches in the SEM picture of the untreated mild steel (Fig. 4). The coated samples' SEM pictures, however (Fig. 5–7) show notable morphological variations. The inclusion of starch caused the grains to become smaller and the structure to become tightly packed. This phenomenon is explained by the electrodeposition process, in which a uniform and compact coating was produced by the applied current mobilizing the distributed ESAp and zinc cations towards the

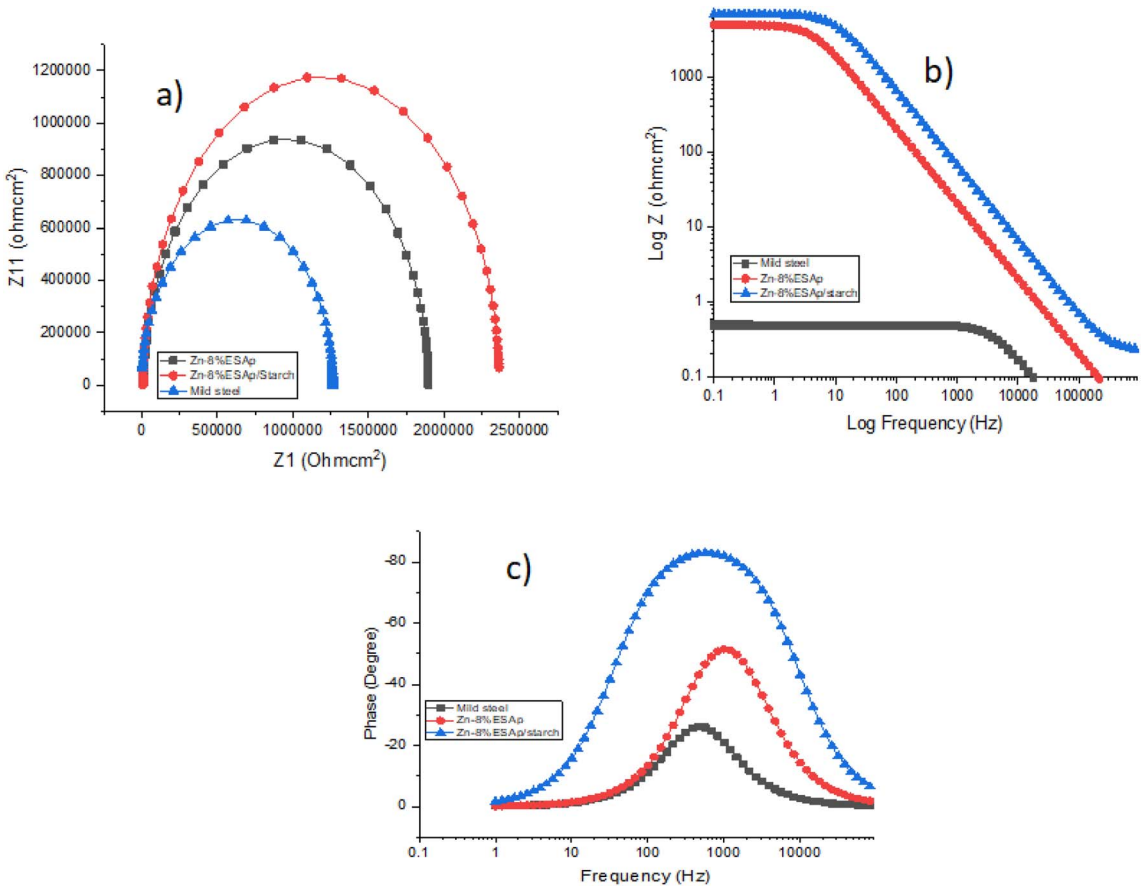

Fig. 12 (a) Nyquist plots (b) Bode impedance plots (c) Bode phase angle plots.

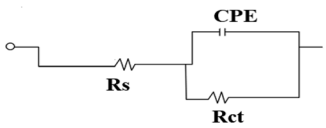

Fig. 13 Equivalent circuit model used to fit the impedance data.

cathodic substrate. The orientation and surface morphology of the coated samples suggest a superior and uniform appearance, which can be linked to the optimized deposition parameters.

The gritty appearance observed during electrodeposition was due to the uniform dispersion of ESAp in the solution. SEM images of the coated samples did not show any external surface defects such as faults, damage, or contours. The characteristics of mild steel are significantly influenced by the surface layers of the coating. The addition of conductive elements such as starch and boric acid is thought to promote adhesion. The Zn-8% ESAp + 2% starch film has superior barrier qualities because it is denser and more compact than the Zn-8% ESAp films, according to SEM examination. These discoveries are in line with the findings of Akpan *et al.*,[49] who found that a fine-grained, homogeneous, and compact microstructure was produced when the Zn–Ni–Al_2O_3 composite was deposited on mild steel.

The composite coating's EDS analysis, shown in Fig. 4–7, adds more credence to these findings. The mild steel substrate's EDS revealed a prominent Fe peak as expected (Fig. 4). However, the coated samples' EDS revealed significant peaks for zinc and calcium, indicating that the coating included these elements from the ESAp (Fig. 5–7). These results confirm the successful integration of ESAp into the coating and show better compositional characteristics of the coated samples, which is in line with the work done by Tuaweri *et al.*[50]

Table 5 EIS results of the composite coating

Sample	R_s	R_{ct} (Ω cm^2)	C_{pdl} (μF cm^{-2})	CPE $\times 10^{-4}$ Ω^{-1} s^n cm^{-2}	$\chi^2 \times 10^{-4}$
Mild steel	3.1×10^2	4.64×10^5	1.91×10^{-9}	8.6	3.5
Zn-8% ESAp	4.6×10^3	1.88×10^6	1.35×10^{-10}	6.4	3.0
Zn-8% ESAp/starch	1.47×10^4	2.35×10^6	6.79×10^{-11}	4.3	2.0

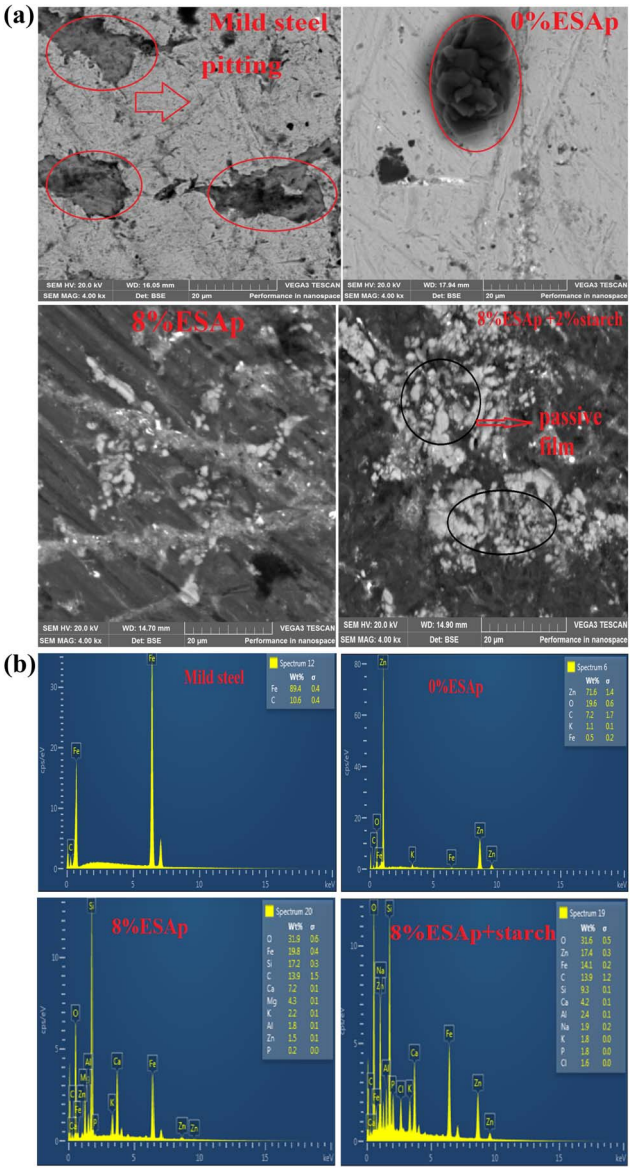

Fig. 14 (a) and (b) SEM corroded images of the samples.

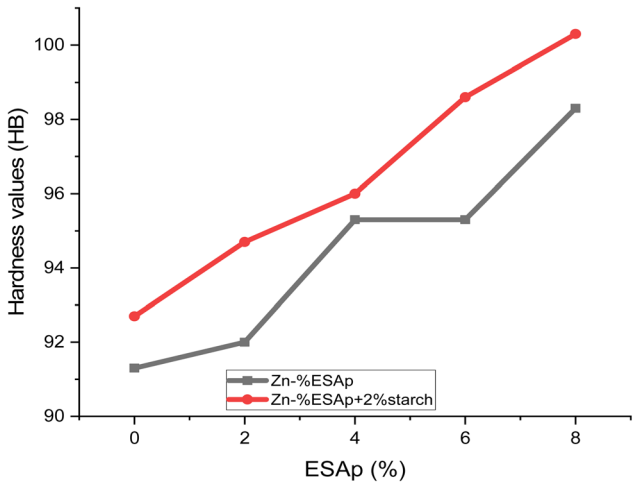

Fig. 15 Variation of hardness values with %ESAp.

3.5. Potential open circuit

The coated samples' anticorrosion performance in a 3.5% NaCl solution at 35 °C was evaluated using open circuit potential (OCP) testing. The results show that the addition of starch and ESAp significantly increased the samples' potential, as seen in Fig. 8 and 9. Surprisingly, the Zn-8% ESAp + 2% starch coating demonstrated enhanced cathodic corrosion shielding ability, as Fig. 9 shows. The formation of surface oxides and other corrosion products contributed to a slight increase in the OCP of the coated samples, leading to a more positive potential value. This shift towards higher positive potential values suggests improved corrosion resistance, attributed to the protective nature of the composite coating and its ability to form stable passive layers on the surface.

However, the barrier effect of Zn and ESAp is responsible for the OCP for the coated samples with starch that retain higher noble potential values than those of Zn-8% ESAp and mild steel. Moreover, Zn and Ca transform into Zn^{2+} and Ca^{2+}, which function as cation ions, in coatings containing Zn and ESAp. The steel substrate's corrosion is halted by these cations. Particularly for Zn-8% ESAp + 2% starch, it was seen that the OCP value shifted in the direction of a nobler value, suggesting improved protective qualities. With a higher positive corrosion potential (E_{corr}) value than the as-received value, the coating was primarily protecting the cathodic area of the steel. Conversely, the Zn-8% ESAp + 2% starch coatings frequently showed a mixed corrosion protection effect. The effect of the starch on the OCP of the steel coatings was further demonstrated by the fact that the OCP, which is a material's initial potential in a corrosive media, remained steady over the 3600 seconds immersion, suggesting that the stable state potential had been attained. However, the OCP of the other samples seemed to vary throughout the course of the 3600 seconds and stabilizations of time was obtained. This is consistent with what Fayomi *et al.*[51] found.

3.6. Polarization *via* potentiodynamics Tafel ellipses

The study examined the protective qualities of various coatings using linear potentiodynamic polarization (Tafel measurements) in a 3.5% NaCl solution. All of the pertinent polarization data, including anodic and cathodic Tafel slopes (b_a, b_c), corrosion potential (E_{corr}), corrosion rate (CR), and current density (I_{corr}), are shown in Fig. 10 and 11. Tafel curves for composite coated electrodes consisting of Zn-%x ESAp ($x = 0$, 2, 4, 6, and 8) and uncoated mild steel are displayed in Fig. 10 and 11. This method was applied to evaluate the degree of corrosion protection offered by various coating film types. The polarization curves of the coated and substrates differed, as seen in Fig. 10 and 11, suggesting varying corrosion tendencies (Table 3).

The whole coated mild steel's corrosion potential (E_{corr}) changed to a noble positive potential, and the coated mild steel electrode's corrosion resistance was significantly reduced.

Additionally, the corrosion current (I_{corr}) was less than that of the electrode made of mild steel. It is commonly recognized that a positive shift in E_{corr} and a decrease in I_{corr} are caused by the Zn layer coating the metal surface. The protection provided by composite coatings is impacted by both the barrier behavior and the passivation effect. According to corrosion kinetics, the rate of corrosion is determined by the corrosion current density; the potential decreases with increasing corrosion resistance. As the corrosion current density increases, so does the corrosion resistance. Consequently, the starch-coated sample exhibits superior resistance to corrosion. The mild steel sample that was obtained exhibited greater corrosion current density (j_{corr}), higher corrosion rate (CR), and lower polarization resistance (PR). When compared to the coated samples, these values showed that the as-received sample had the lowest resistance to the corrosive medium's degrading impact (3.65% NaCl). ESp coating significantly raised PR while lowering CR and j_{corr}.

This response showed that the coated sample was being kept free of chloride ions by the ESA particles. In contrast to the Zn-8% ESAp sample, the Zn-8% ESAp + 2% starch coated sample had lower CR and j_{corr} values when it came to corrosion resistance performance (Table 4 and Fig. 11). At Zn-8% ESAp and Zn-8% ESAp + 2% starch, corrosion protection efficiencies of 82.92 and 94.69% were attained. The addition of Zn–Zn-8% ESAp + 2% starch enhanced the adhesive binding of the coating by reducing the amount of holes or pores that the corrosive medium may penetrate, as shown by the decreased corrosion resistance. Furthermore, it's likely that the 2% starch added to the Zn-% ESAp coating matrix inhibited the growth of the micro-voids in the ESA particles, shrank the diameters and boundaries of the grains, and hampered the production of new grains. Higher CR and j_{corr} values may have been the outcome, though, if the reduced quantity of ESA had reinforced big grain boundaries and created more gaps, apertures, or holes for the chloride ions to flow through. It is evident that the results obtained with the starch modifier show lower passivation current and oxide monomer current density than those obtained without it. This suggests that a less conductive composite coating with improved protective properties has been produced.

Zn–Zn-8% ESAp + 2% starch has been discovered to have the greatest polarization resistance and lower corrosion current, indicating superior protective characteristics.[52] Barrier effects and electrochemical protection are said to be the two most crucial elements in improving the corrosion-resistant properties of composite coatings. Put another way, the electrochemical protection justifies the formation of a passive layer on the metal surface and the increase in corrosion potential. Furthermore, since starch plays a useful function in dispersing Zn and ESAp to generate a thick and smooth coating surface, mild steel has been provided advantageous morphological qualities to protect it from corrosive environments by the Zn-8% ESAp + 2% starch coating.

3.7. Electrochemical impedance spectroscopy (EIS)

The effectiveness of the composite coating under research in preventing corrosion while submerged in a 3.5% NaCl solution was verified using EIS. Fig. 12 presents the EIS spectra, including both Bode and Nyquist plots, for mild steel, Zn-8% ESAp, and Zn-8% ESAp/starch samples. The single capacitive loop displayed in the Nyquist plot (Fig. 12a) illustrates the charge transfer occurring during the corrosion process. The significantly larger diameter of the loop for the Zn-8% ESAp/starch-coated sample indicates that the composite coating offers higher resistance, attributed to the enhanced surface coverage provided by the starch.

The sample containing starch exhibited a greater semicircle diameter compared to the one without starch. A larger semicircle diameter, or more pronounced persistence of charge transfer, is often indicative of higher corrosion resistance.[50] The increase in charge transfer resistance is believed to result from the corrosion products formed on the sample surface, which reduce the corrosion rate.[34,50] The Zn-8% ESAp/starch sample demonstrated the highest corrosion resistance, evidenced by the widest capacitive arc width. This enhancement is attributed to the formation of a barrier between the corrosive electrolyte and the sample surface, where the resulting oxide layer passively increases the material's resistance to corrosion.

The formation of an oxide layer is evident from the semicircle loop in the Nyquist plot, which suggests a strong protective effect of the passive layer. However, the presence of an inductance loop indicates potential delamination of the passive layer. Fig. 13 illustrates the impedance plots fitted with an equivalent circuit comprising solution resistance (R_s), charge transfer resistance (R_{ct}), and double-layer capacitance (C_{dl}). To achieve a more accurate fit, the double-layer capacitance (C_{dl}) is replaced by a constant phase element (CPE), as the metal/solution interface does not behave as an ideal capacitor.

Table 5 summarizes the EIS parameters, including R_s, R_{ct}, and C_{dl}. Typically, a decrease in C_{dl} values combined with an increase in R_{ct} values signifies improved surface coverage and enhanced corrosion prevention. This is further supported by the Bode diagrams. The Bode modulus diagram shows an increase in impedance modulus across all frequencies, while the Bode phase angle diagram displays a more negative phase angle at high frequencies, indicating the beneficial effect of starch. The charge transfer resistance (R_{ct}) is a crucial parameter for assessing the effectiveness of the passive layer. Higher R_{ct} values denote greater resistance to ion movement within the passive layer, leading to better corrosion resistance. Fig. 12a shows that mild steel exhibits smaller semi-conductive loops compared to the coated samples, indicating that Zn-8% ESAp/starch coatings provide superior passive layer barrier efficiency.

The chi-square (χ^2) values confirm the fitting accuracy of the equivalent circuit. Values of χ^2 around 10^{-3} typically indicate a good fit,[51] and the relatively low χ^2 values ($<10^{-3}$) for the proposed equivalent circuit in Table 5 suggest that the observed impedance spectra fit well with the suggested model.

Overall, the addition of starch enhances corrosion resistance, likely due to the electron-rich heteroatoms in starch, which facilitate the adsorption of ESAp on the metal surface during electrodeposition, thereby increasing the coating's surface coverage and improving its protective capabilities.[45]

3.8. SEM corrosion surface

The corroded surface of the substrate and its composite covering were examined using a scanning electron microscope. The substrate was shown to have a higher tendency to pit than the samples that were covered. Many of the pits had an iron oxide covering surrounding them, indicating that pit formation continues during the exposure time as iron oxide accumulates on the surface (Fig. 14a).

The eroding surface of the coated material demonstrated that the mild steel's surface had retained the Zn and ESAp in the absence of corrosion attack. By covering the surface of the mild steel, the coating functions as a passive corrosion barrier. The presence of hard phases in the Zn-ESAp composite coating samples reduces the degree and kind of surface damage. Zn-8% ESAp + 2% starch stems exhibited less overall damage because the hard phases shield the stems from the damaging effects of the corrosion. Consequently, this result confirms that the essence of ESAp allows for reduced sample degradation. Moreover, the corrosion process would be slowed down since the superior dispersion of Zn and ESAp that starch promised assisted in sealing the coating's pores and limiting the paths that corrosive ions and the electrolyte might take.

Fig. 14b displays the corroded samples' EDS. It was evidence that Fe, C, and O were the visible elements in mild steel; however, the corroded sample containing only Zn with the absence of starch and ESAp show Fe, Zn, C, O, and Cl. Why the coated samples containing 8% ESAp and 8% ESAp + starch reveal Fe, Zn, C, O, Cl, Si, Ca, and Na. Compared to the other studied samples, the 8% ESAp + starch sample exhibits more diffraction peaks. This backs up the early findings that the 8% ESAp + starch sample formed more corrosion products that prevent the mild steel from further corrosion attack. The corroded product that forms may be ZnO, $Zn(OH)_2$, CaO, $CaCO_3$, and Na_2O. Work by[25,28] has yielded similar observations. It was evident that the corrosion attack had caused a significant variation in the EDS spectrum between the samples under investigation. The different oxide layers emerge, which help to form a thin film around the materials and halt further corrosion attacks on the 8% ESAp + starch sample was responsible for the lowest corrosion rate.

3.9. Hardness values

Fig. 15 displays the Brinell hardness of the coated and as-received samples. The mild steel sample has the lowest Brinell hardness rating when compared to the other samples. This demonstrated that obtaining the indenting force on the steel ball was facilitated by the sample. It was discovered that the Zn-8% ESAp + %starch coated steel had a much greater Brinell hardness than the sample that was received. The Brinell hardness of the Zn-8% ESAp + %starch-coated steel sample was 100.3, indicating a 46.45% improvement in hardness. The capacity of ESAp to disperse, harden, and refine grain within the coating matrix might account for the extraordinary hardness of the Zn-8% ESAp + %starch coating.[53] It's possible that trace elements like calcium found in the ESA particles worked with Zn to create a layer of reinforcement between the coating and steel. Consequently, the coated steel's plastic deformation was reduced by the hardened layer.

4. Conclusion

The study successfully developed Zn-*X*%ESAp (0, 2, 4, 6, and 8) coatings with starch extract as a modifier, demonstrating significant improvements in the anti-corrosion behavior of mild steel. The Zn-ESAp + 2% starch coatings were effectively applied, with coating thickness increasing proportionally to the ESAp content. SEM analysis revealed no external surface defects, indicating a high-quality coating process. Notably, the Zn-8% ESAp + 2% starch-coated sample exhibited a 46.45% increase in hardness, reaching 100.3 HB, and achieved impressive corrosion protection efficiencies of 82.92% and 94.69% for Zn-8% ESAp and Zn-8% ESAp + 2% starch, respectively. The coated samples showed a shift towards greater positive potential, enhancing their corrosion resistance compared to untreated mild steel. Overall, the Zn-8% ESAp + 2% starch composite was identified as having the optimum properties for anti-corrosion applications, demonstrating the effective use of starch extract and eggshell particles in improving the durability and performance of mild steel coatings.

Acceptance of ethics

Because this experiment does not involve people or animals, no ethics committee approval is required.

Consent of participants

Because this study does not include people or animals, no permission is required to participate.

Publishing permission

The writers grant their permission for the work to be published by the publisher.

Consent to publish

The author gives the publisher the consent to publish the work.

Data availability

The author confirm that the data supporting this study's conclusions is included in the publication.

Author contributions

All contributed 100 percent to the study's development, from experimentation to analysis.

Conflicts of interest

There is no conflicts of interest in this work.

Acknowledgements

The authors hereby appreciates and acknowledges the Africa Centre of Excellence for Sustainable Power and Energy Development, ACE-SPED, University of Nigeria, Nsukka; Energy materials research group, University of Nigeria, Nsukka, Nigeria; and Faculty of Engineering and Built Environment, University of Johannesburg, Auckland Park, South Africa for their supports.

References

1 R. Bender, D. Féron, D. Mills, S. Ritter, R. Bäßler, D. Bettge, I. De Graeve, A. Dugstad, S. Grassini, T. Hack and M. Halama, Corrosion challenges towards a sustainable society, *Mater. Corros.*, 2022, **73**(11), 1730–1751.

2 C. Verma, D. S. Chauhan, R. Aslam, P. Banerjee, J. Aslam, T. W. Quadri, S. Zehra, D. K. Verma, M. A. Quraishi, S. Dubey and A. AlFantazi, Principles and theories of green chemistry for corrosion science and engineering: design and application, *Green Chem.*, 2024, **26**(8), 4270–4357.

3 D. Raabe, The materials science behind sustainable metals and alloys, *Chem. Rev.*, 2023, **123**(5), 2436–2608.

4 H. S. Aljibori, A. Alamiery and A. A. Kadhum, Advances in corrosion protection coatings: A comprehensive review, *Int. J. Corros. Scale Inhib.*, 2023, **12**(4), 1476–1520.

5 M. Vakili, P. Koutník and J. Kohout, Addressing hydrogen sulfide corrosion in oil and gas industries: A sustainable perspective, *Sustainability*, 2024, **16**(4), 1661.

6 K. Bijapur, V. Molahalli, A. Shetty, A. Toghan, P. De Padova and G. Hegde, Recent trends and progress in corrosion inhibitors and electrochemical evaluation, *Appl. Sci.*, 2023, **13**(18), 10107.

7 N. Eliaz, Corrosion of metallic biomaterials: A review, *Materials*, 2019, **12**(3), 407.

8 I. P. Okokpujie, L. K. Tartibu, H. O. Musa-Basheer and A. O. M. Adeoye, Effect of coatings on mechanical, corrosion and tribological properties of industrial materials: a comprehensive review, *J. Bio- Tribo-Corros.*, 2024, **10**(1), 2.

9 H. Zhu and J. Li, Advancements in corrosion protection for aerospace aluminum alloys through surface treatment, *Int. J. Electrochem. Sci.*, 2024, 100487, DOI: **10.1016/j.ijoes.2024.100487**.

10 A. R. Prasad, A. Kunyankandy and A. Joseph, Corrosion inhibition in oil and gas industry: Economic considerations, *Corrosion Inhibitors in the Oil and Gas Industry*, 2020, pp. 135–150.

11 M. Iannuzzi and G. S. Frankel, The carbon footprint of steel corrosion, *npj Mater. Degrad.*, 2022, **6**(1), 101.

12 A. Thakur,P. K. Sharma and A. Kumar, Economics and commercialization of carbon allotropes nanostructured corrosion inhibitors. *Carbon Allotropes: Nanostructured Anti-Corrosive Materials*, 2022, vol. 383.

13 M. Zubielewicz, E. Langer, A. Królikowska, L. Komorowski, M. Wanner, K. Krawczyk, L. Aktas and M. Hilt, Concepts of steel protection by coatings with a reduced content of zinc pigments, *Prog. Org. Coat.*, 2021, **161**, 106471.

14 R. Somoghi, V. Purcar, E. Alexandrescu, I. C. Gifu, C. M. Ninciuleanu, C. M. Cotrut, F. Oancea and H. Stroescu, Synthesis of zinc oxide nanomaterials via sol-gel process with anti-corrosive effect for Cu, Al and Zn metallic substrates, *Coatings*, 2021, **11**(4), 444.

15 R. Rohani, N. S. Dzulkharnien, N. H. Harun and I. A. Ilias, Green approaches, potentials, and applications of zinc oxide nanoparticles in surface coatings and films, *Bioinorg. Chem. Appl.*, 2022, **2022**(1), 3077747.

16 A. K. Hussain, N. Seetharamaiah, M. Pichumani and C. S. Chakra, Research progress in organic zinc rich primer coatings for cathodic protection of metals–A comprehensive review, *Prog. Org. Coat.*, 2021, **153**, 106040.

17 V. P. Hoang Huy, L. T. Hieu and J. Hur, Zn metal anodes for Zn-ion batteries in mild aqueous electrolytes: Challenges and strategies, *Nanomaterials*, 2021, **11**(10), 2746.

18 P. P. Wu, G. L. Song, Y. X. Zhu and D. J. Zheng, Intelligentization of traditional sacrificial anode Zn by Mg-alloying for reinforcing steel, *Corros. Sci.*, 2022, **194**, 109943.

19 A. Dan, P. K. Bijalwan, A. S. Pathak and A. N. Bhagat, A review on physical vapor deposition-based metallic coatings on steel as an alternative to conventional galvanized coatings, *J. Coat. Technol. Res.*, 2022, **19**(2), 403–438.

20 D. Lin, X. Wang, M. Zhang, S. Yuan, F. Xu, D. Bao and H. Wang, A robust and eco-friendly waterborne anti-corrosion composite coating with multiple synergistic corrosion protections, *Composites, Part B*, 2022, **232**, 109624.

21 Z. Bai, S. Meng, Y. Cui, Y. Sun, L. Pei, H. Hu, Y. Jiang and H. Wang, A stable anticorrosion coating with multifunctional linkage against seawater corrosion, *Composites, Part B*, 2023, **259**, 110733.

22 W. M. Kamaruzzaman, M. S. Shaifudin, N. A. Nasir, N. A. Hamidi, N. Yusof, A. Adnan, L. O. Jew, W. M. Nik and M. S. Ghazali, Eggshells biowaste filler for improving the anticorrosive behaviour of waterborne polyurethane coatings on mild steel in artificial seawater, *J. Mater. Res. Technol.*, 2022, **21**, 3815–3827.

23 A. Zamani, S. Eavani and E. Rafiee, Synthesis and characterization of anticorrosion, low-lead leaching PbCrO4/eggshell composites as the environmentally sustainable yellow pigments, *J. Cleaner Prod.*, 2021, **304**, 127103.

24 O. Sanni, S. A. Iwarere and M. O. Daramola, Investigation of eggshell agro-industrial waste as a potential corrosion inhibitor for mild steel in oil and gas industry, *Sustainability*, 2023, **15**(7), 6155.

25 E. Atikpo, V. S. Aigbodion and D. V. Von Kallon, $CaCO_3$-derived from eggshell waste for improving the corrosion resistance of zinc composite coating on mild steel for biodiesel storage tank, *Chem. Data Collect.*, 2022, **37**, 100794.

26 Y. Wen, H. Qing, H. Shu and Q. Liu, Evaluating the protective effects of calcium carbonate coating on sandstone cultural heritage, *Coatings*, 2021, **11**(12), 1534.

27 J. Guo, X. Li, Y. Xu, P. Zhang and K. Wang, Neutralization evolution of concrete under acid rain and carbonation erosion: A review, *J. Mater. Res. Technol.*, 2023, **25**, 1376–1405.

28 V. S. Aigbodion and E. T. Akinlabi, Explicit microstructural evolution and electrochemical performance of zinc-eggshell particles composite coating on mild steel, *Surf. Interfaces*, 2019, **17**, 100387.
29 Z. Pu, X. Jing, C. Yang, F. Wang and K. F. Ehmann, Wettability modification of zirconia by laser surface texturing and silanization, *Int. J. Appl. Ceram. Technol.*, 2020, **17**(5), 2182–2192.
30 H. Riazi, M. Anayee, K. Hantanasirisakul, A. A. Shamsabadi, B. Anasori, Y. Gogotsi and M. Soroush, Surface modification of a MXene by an aminosilane coupling agent, *Adv. Mater. Interfaces*, 2020, **7**(6), 1902008.
31 C. Calvino, N. Macke, R. Kato and S. J. Rowan, Development, processing and applications of bio-sourced cellulose nanocrystal composites, *Prog. Polym. Sci.*, 2020, **103**, 101221.
32 M. R. Azani and A. Hassanpour, Nanotechnology in the fabrication of advanced paints and coatings: dispersion and stabilization mechanisms for enhanced performance, *ChemistrySelect*, 2024, **9**(19), e202400844.
33 T. A. Nguyen and T. T. Bui, Study the effects of carbon nanotubes and graphene oxide combinations on the mechanical properties and flame retardance of epoxy nanocomposites, *J. Nanomater.*, 2021, **2021**(1), 1437929.
34 Z. Shahryari, M. Yeganeh, K. Gheisari and B. A. Ramezanzadeh B, A brief review of the graphene oxide-based polymer nanocomposite coatings: preparation, characterization, and properties, *J. Coat. Technol. Res.*, 2021, **18**(4), 945–969.
35 A. Kumar, K. Sharma and A. R. Dixit, A review on the mechanical properties of polymer composites reinforced by carbon nanotubes and graphene, *Carbon Lett.*, 2021, **31**(2), 149–165.
36 C. Guo, J. Liu, X. Li and S. Yang, Effect of cavitation bubble on the dispersion of magnetorheological polishing fluid under ultrasonic preparation, *Ultrason. Sonochem.*, 2021, **79**, 105782.
37 D. H. Sung, S. M. Doshi, C. Murray, A. N. Rider and E. T. Thostenson, Electrophoretic deposition: Novel in situ film growth mechanism of carbon nanocomposite films within non-conductive fabrics for multi-scale hybrid composites, *Compos. Sci. Technol.*, 2020, **200**, 108415.
38 D. H. Sung, S. M. Doshi, A. N. Rider and E. T. Thostenson, Innovative alternating current electrophoretic deposition for micro/nanoscale structure control of composites, *ACS Appl. Electron. Mater.*, 2023, **5**(7), 3715–3725.
39 X. Cheng, Y. Liu, O. Liu, Y. Lu, Z. Liao, Z. Hadzhieva, L. Chen, S. G. Leeuwenburgh, A. R. Boccaccini and F. Yang, Electrophoretic deposition of coatings for local delivery of therapeutic agents, *Prog. Mater. Sci.*, 2023, **14**, 101111.
40 M. Atiq Ur Rehman, Q. Chen, A. Braem, M. S. Shaffer and A. R. Boccaccini, Electrophoretic deposition of carbon nanotubes: recent progress and remaining challenges, *Int. Mater. Rev.*, 2021, **66**(8), 533–562.
41 M. Kaseem and Y. G. Ko, Effect of starch on the corrosion behavior of Al-Mg-Si alloy processed by micro arc oxidation from an ecofriendly electrolyte system, *Bioelectrochem*, 2019, **128**, 133–139.
42 O. D. Akinfenwa, O. S. Fayomi, J. O. Atiba and B. E. Anyaegbuna, Development of starch-modified titanium oxide paired with zinc powder using the electrodeposition technique as a composite superhydrophobic coating for mild steel, *Int. J. Adv. Manuf. Technol.*, 2024, **130**(5), 2847–2854.
43 F. C. Walsh, S. Wang and N. Zhou, The electrodeposition of composite coatings: Diversity, applications and challenges, *Curr. Opin. Electrochem.*, 2020, **20**, 8–19.
44 M. Aliofkhazraei, F. C. Walsh, G. Zangari, H. Köçkar, M. Alper, C. Rizal, L. Magagnin, V. Protsenko, R. Arunachalam, A. Rezvanian and A. Moein, Development of electrodeposited multilayer coatings: A review of fabrication, microstructure, properties and applications, *Appl. Surf. Sci. Adv.*, 2021, **6**, 100141.
45 A. B. Nandiyanto, T. Rahman, M. A. Fadhlulloh, A. G. Abdullah, I. Hamidah and B. Mulyanti, Synthesis of silica particles from rice straw waste using a simple extraction method, *IOP Conf. Ser.: Mater. Sci. Eng.*, 2016, **128**(1), 012040.
46 E. A. Wibowo, A. W. Arzanto, K. D. Maulana, I. S. Hardyanti, H. D. Septyaningsih and N. Widiarti, Preparation and characterization of silica nanoparticles from rice straw ash and its application as fertilizer, *J. Chem. Pharm. Res.*, 2017, **9**, 193–199.
47 O. S. I. Fayomi, A. P. I. Popoola and V. S. Aigbodion, Effect of thermal treatment on the interfacial reaction, microstructural and mechanical properties of Zn–Al–SnO_2/TiO_2 functional coating alloys, *J. Alloys Compd.*, 2014, **617**, 455–463.
48 V. S. Aigbodion, S. I. Neife and I. Y. Suleiman, Surface modification of mild steel by co-deposition using Zn-ZnO-Ant hill particulate composite coating in simulated sea water, *Proc. Inst. Mech. Eng. M: J. Eng. Marit. Environ.*, 2019, **233**(3), 857–867.
49 B. J. Akpan, I. G. Akande, O. S. Fayomi and K. M. Oluwasegun, Investigation of hardness, microstructure and anti-corrosion properties of Zn-ZnO composite coating doped unripe plantain peel particles, *Case Stud. Chem. Environ. Eng.*, 2022, **5**, 100187.
50 T. J. Tuaweri, E. M. Adigio and P. P. Jombo, A study of process parameters for zinc electrodeposition from a sulphate bath, *Int. J. Eng. Sci.*, 2013, **2**(8), 17–24.
51 O. S. Fayomi, A. P. Popoola and V. S. Aigbodion, Investigation on microstructural, anti-corrosion and mechanical properties of doped Zn–Al–SnO_2 metal matrix composite coating on mild steel, *J. Alloys Compd.*, 2015, **623**, 328–334.
52 Z. Sharifalhoseini, M. H. Entezari and M. Shahidi, Direct growth of ZnO nanostructures on the Zn electroplated mild steel to create the surface roughness and improve the corrosion protection of the electroless Ni-P coating, *Mater. Sci. Eng. B.*, 2018, **231**, 18–27.
53 A. Kherfi, A. Madani, D. Chalal and S. Benidir, Improvement of the protective properties of the nanocomposite polypyrrole-zinc oxide coating on mild steel by adding the dispersant sodium hexametaphosphate, *Synth. Met.*, 2021, **277**, 116795.